NASA/TM—1999-208855

High Temperature Mechanical Characterization and Analysis of Al_2O_3/Al_2O_3 Composites

John Z. Gyekenyesi
University of Akron, Akron, Ohio

Martha H. Jaskowiak
Lewis Research Center, Cleveland, Ohio

February 1999

The NASA STI Program Office . . . in Profile

Since its founding, NASA has been dedicated to the advancement of aeronautics and space science. The NASA Scientific and Technical Information (STI) Program Office plays a key part in helping NASA maintain this important role.

The NASA STI Program Office is operated by Langley Research Center, the Lead Center for NASA's scientific and technical information. The NASA STI Program Office provides access to the NASA STI Database, the largest collection of aeronautical and space science STI in the world. The Program Office is also NASA's institutional mechanism for disseminating the results of its research and development activities. These results are published by NASA in the NASA STI Report Series, which includes the following report types:

- TECHNICAL PUBLICATION. Reports of completed research or a major significant phase of research that present the results of NASA programs and include extensive data or theoretical analysis. Includes compilations of significant scientific and technical data and information deemed to be of continuing reference value. NASA's counterpart of peer-reviewed formal professional papers but has less stringent limitations on manuscript length and extent of graphic presentations.

- TECHNICAL MEMORANDUM. Scientific and technical findings that are preliminary or of specialized interest, e.g., quick release reports, working papers, and bibliographies that contain minimal annotation. Does not contain extensive analysis.

- CONTRACTOR REPORT. Scientific and technical findings by NASA-sponsored contractors and grantees.

- CONFERENCE PUBLICATION. Collected papers from scientific and technical conferences, symposia, seminars, or other meetings sponsored or cosponsored by NASA.

- SPECIAL PUBLICATION. Scientific, technical, or historical information from NASA programs, projects, and missions, often concerned with subjects having substantial public interest.

- TECHNICAL TRANSLATION. English-language translations of foreign scientific and technical material pertinent to NASA's mission.

Specialized services that complement the STI Program Office's diverse offerings include creating custom thesauri, building customized data bases, organizing and publishing research results . . . even providing videos.

For more information about the NASA STI Program Office, see the following:

- Access the NASA STI Program Home Page at ***http://www.sti.nasa.gov***

- E-mail your question via the Internet to help@sti.nasa.gov

- Fax your question to the NASA Access Help Desk at (301) 621-0134

- Telephone the NASA Access Help Desk at (301) 621-0390

- Write to:
  NASA Access Help Desk
  NASA Center for AeroSpace Information
  7121 Standard Drive
  Hanover, MD 21076

NASA/TM—1999-208855

High Temperature Mechanical Characterization and Analysis of $A1_2O_3/A1_2O_3$ Composites

John Z. Gyekenyesi
University of Akron, Akron, Ohio

Martha H. Jaskowiak
Lewis Research Center, Cleveland, Ohio

National Aeronautics and
Space Administration

Lewis Research Center

February 1999

Acknowledgments

We would like to thank Mr. John A. Setlock of Case Western Reserve University (CWRU) for the processing of the specimens, scanning electron microscopy, and fiber test data. Also, we would like to thank Dr. Ali Sayir of CWRU for the high temperature fiber moduli data used in this paper.

High Temperature Mechanical Characterization and Analysis of Al_2O_3/Al_2O_3 Composites

John Z. Gyekenyesi
University of Akron
Civil Engineering Department
Akron, Ohio

and

Martha H. Jaskowiak
NASA Lewis Research Center
Cleveland, Ohio

Abstract

Sixteen ply unidirectional zirconia coated single crystal Al_2O_3 fiber reinforced polycrystalline Al_2O_3 was tested in uniaxial tension at temperatures to 1400°C in air. Fiber volume fractions ranged from 26 to 31%. The matrix has primarily open porosity of approximately 40%. Theories for predicting the Young's modulus, first matrix cracking stress, and ultimate strength were applied and evaluated for suitability in predicting the mechanical behavior of Al_2O_3/Al_2O_3 composites.

The composite exhibited pseudo tough behavior (increased area under the stress/strain curve relative to monolithic alumina) from 22° to 1400°C. The rule-of-mixtures provides a good estimate of the Young's modulus of the composite using the constituent properties from room temperature to approximately 1200°C for short term static tensile tests in air. The ACK theory provides the best approximation of the first matrix cracking stress while accounting for residual stresses at room temperature. Difficulties in determining the fiber/matrix interfacial shear stress at high temperatures prevented the accurate prediction of the first matrix cracking stress above room temperature. The theory of Cao and Thouless, based on Weibull statistics, gave the best prediction for the composite ultimate tensile strength.

1. Introduction

Ceramics in general are extremely brittle, have low strain tolerance, and exhibit a wide variation in ultimate strength. The observed scatter in strength is caused by an abundance of imperfections, i.e., flaws, that are a result of material processing. Over the years, the strength reliability of monolithic ceramics have improved as better processing techniques have evolved. However, as Dev (1992), Taylor (1991), and Zweben (1998) indicate, the brittle failure characteristics of these materials make them acceptable in only a limited range of applications. Even in the limited structural application of monolithic ceramics to turbines in automotive turbochargers, turbo efficiency is sacrificed for structural reliability as noted by Yoshida and Kokji (1989). In an effort to increase ceramic toughness and strength, ceramic matrix composites with various reinforcements are being developed. These developments are covered briefly by King (1989) and Levine (1992). These composites may include multiple phases or matrices with particulates, whiskers, or continuous fibers.

In the gas turbine industry, ceramic matrix composites (CMCs) are particularly attractive since they have the potential to replace nickel based superalloys in various hot section components (Dix and Petty (1990) and Constance (1990)). The primary attribute of CMCs relative to nickel based superalloys is the ability of CMCs to be used well beyond current turbine service temperatures, as well as to withstand more severe operating environments. This would enable engines to be operated at higher temperatures with near-stoichiometric combustion without cooling air requirement penalties as noted by Drascovich (1993). Increasing operating temperature is a classic approach for improving turbine efficiency. Zweben (1998) notes that the low density and high temperature properties of CMCs make them potential materials in hot structures and propulsion systems of reusable launch vehicles.

Another attraction of ceramic composites is their relative low density, which is, as Holmes and Wu (1995) point out, typically 65% to 75% lower than conventional superalloys. One can not overemphasize the fact that weight is a critical design facet for gas turbines utilized in aeropropulsion. Lastly, CMCs offer the potential of increased durability, relative to superalloys, at the high operating temperatures. This would result in increased time between engine overhauls reducing operating costs.

In virtually all ceramic matrix composite systems the goal of the materials scientist is to apply a closing pressure on existing matrix crack surfaces and to impart a tortuous fracture path by crack deflection. This results in an increase in the apparent toughness of the material as noted by Warren (1992). Unlike polymer and metal matrix composites, the fiber/matrix interface in a fiber reinforced ceramic composite must be relatively weak. Optimization of the interface prevents matrix cracks from propagating through the fibers while still providing load transfer. As a result, unbroken fibers bridge a propagating matrix crack, which increases the composite work of fracture. In essence, the fiber/matrix interface has to be strong enough to allow load transfer and retain acceptable strength in the transverse direction, but the interface must also allow debonding as a crack passes around the fiber.

There are many ceramic matrix composite systems being investigated and developed, as indicated by Sheppard (1992) and Studt (1991). One of these systems consists of zirconia coated continuous single crystal alumina fibers and an alumina matrix (Al_2O_3/Al_2O_3). As an oxide, these composites don't have the oxidation problems of silicon based ceramics.

The path to successful commercialization of the CMC systems mentioned above must include the characterization and evaluation of engineering design properties. As Duffy and Gyekenyesi (1995) point out this requires characterization of mechanical and thermal properties. It is essential to characterize the creep behavior of these materials as well as ascertain how temperature affects their fast fracture. Motivated by the general lack of high quality test data required by the design engineer, this paper presents high-temperature, fast fracture data of the aforementioned Al_2O_3/Al_2O_3 composite. This data was acquired using a high temperature tensile testing facility assembled by Gyekenyesi (1998) at NASA LeRC. The properties of these material systems were obtained in the primary fiber direction.

The objective of this paper is to determine selected CMC mechanical properties and predict the mechanical behavior with existing theoretical models. Flat Al_2O_3/Al_2O_3 composite specimens were tested. The continuous monofilament fibers in the composite were oriented in the primary direction, which presents an upper bound for strength, stiffness, and work of fracture properties for this composite system.

For this study unidirectional Al_2O_3/Al_2O_3 composites were tested from room temperature to 1400°C (2550°F) in air. The experimental data were compared with theoretical predictions for stiffness, proportional limit or first matrix cracking stress, and ultimate strength.

2. Equipment

The tensile test equipment used for this experiment was setup to test flat ceramic matrix composites at temperatures to 1500°C (2730°F) in air. Most of the equipment was previously described by Gyekenyesi (1998), with the exception of a new furnace and grips that have been incorporated since then. A brief summary is presented here.

The universal tensile testing frame has a mechanical central screw actuator. The machine's actuator has a 100 kN (22 kip) load capacity and a displacement range of 100 mm (4 in.). It is digitally controlled, allowing closed-loop control with load, strain, or crosshead displacement.

A 50 kN (11 kip) load cell was used with the frame. The load cell's output was calibrated such that 10 volts corresponded with a 20 kN (4.5 kips) load. This output was used as input for the computerized data acquisition system.

Water cooled, hydraulically actuated wedge grips were used to hold the specimen in the test frame. These grips are mounted to a rigid load train with a permanent alignment device. The grip faces have a grit surface. Thermocouples are fastened to the grip faces to monitor the temperature near the ends of the specimen.

A low contact force mechanical extensometer was utilized for the high temperature tests to measure axial strain. This device employs a variable capacitor to convert displacements into electrical signals. Low contact forces minimize the bending in test specimens. The silicon carbide rods with knife edges are gas cooled along with the body of the extensometer. The gage length is fixed at 25 mm (0.98 in.).

A clip-on extensometer was used for the room temperature tests to measure axial strain. The gage works in conjunction with the frame's electronic controls. As a result, the frame's controls are used to electronically calibrate the gage and process its signal. The gage has a fixed gage length of 12.7 mm (0.5 in.) with a 12.7 mm (0.5 in.) extender for a total gage length of 25.4 mm (1.0 in.). The maximum extension of this gage is ±1.27 mm (±0.05 in.). This results in a maximum strain range of ±5.0%. Rubber bands were used to hold the gage to the specimen.

Specimen heating was accomplished with the use of an induction heating system and a recrystalized silicon carbide cylindrical susceptor. The susceptor has a 51 mm (2.00 in.) inner diameter with a 60 mm (2.38 in.) outer diameter. The furnace is similar to the system presented by Worthem and Lewinsohn (1991) with the exception that the power supply is a slightly smaller bench top model. The specimen is passed through open slots in the side of the susceptor. The extensometer rods pass through another slot. The ends of the cylinder are plugged with silicon carbide disks. A thermocouple, placed near the specimen surface is used to monitor the gage section temperature.

Lastly, a computerized data acquisition and analysis system was used to collect the test data. The software also was used to determine various material properties from the collected data.

3. Test Specimen Configuration

The Al_2O_3/Al_2O_3 composite specimens had a fiber volume fraction ranging from 26% to 31%. Fibers consisted of uniaxially aligned single crystal alumina fibers. The matrix was polycrystalline alumina with primarily open porosity of 40%. The specimen geometry consisted of 16 plies. The fabrication of the composite is summarized by Jaskowiak, et al. (1997).

The C-axis sapphire fibers have a mean diameter of 132 microns (5.2 mils). An unstabilized zirconia coating of 1.5 to 2.0 μm (59-79 μin.) was applied to the fibers to act as an interface between the fibers and the matrix. The zirconia coating has a similar porosity to that of the alumina of the matrix. The resulting volume fraction of the interface is slightly greater than 1% of the composite.

The composite specimens used in this research were flat, constant thickness, straight sided coupons with bonded tabs on either end. Glass fiber/epoxy composite tabs were used for room temperature tests, and carbon fiber/polyimide composite tabs were utilized in high temperature tests. These tabs provided a compliant layer between the specimen and the grip faces. The tabs were bonded to the specimen using structural film adhesives. The structural film adhesives require curing temperatures of 120°C (250°F) and 180°C (350°F) for the room temperature and high temperature specimens, respectively.

Specimen lengths were 152 mm (6.0 in.). The specimen width was approximately 13 mm (0.5 in.) for all tests. The thickness was approximately 1.7 mm (0.07 in.). Tensile coupons were cut from a panel with a diamond impregnated abrasive wheel.

The specimen geometry was designed based on the American Society for Testing and Materials (ASTM) Standard C 1359-96. The specimen geometry is shown in Figure 1. ASTM Standard C 1359-96 is a recently developed standard test method for obtaining tensile properties of continuous fiber-reinforced ceramics with rectangular cross-sections at high temperatures. The configuration has been used successfully in the past with failures usually occurring within the gage section. In this research effort the carbon fiber/polyimide composite tabs were 32 mm (1.25 in.) long, 13 mm (0.5 in.) wide, and 1.5 mm (0.060 in.) thick.

In addition to the composite specimens, monolithic alumina coupons were fabricated. These specimens had the same geometry as the composite coupons, that is, straight sided flat coupons with bonded tabs on each end. Each coupon was 152 mm (6.0 in.) long with a width of 13 mm (0.5 in.).

4. Procedure

Due to the limited availability of ceramic composite specimens, only two to four coupons were used for each of the test conditions.

The room temperature tests utilized clip-on gages. The clip-on gages were shunt calibrated using the tensile testing frame's controls. The gage was calibrated such that 5.0 percent strain resulted in a 10 volt output. The gage was used with the 25 mm (1.0 in.) gage length. The high

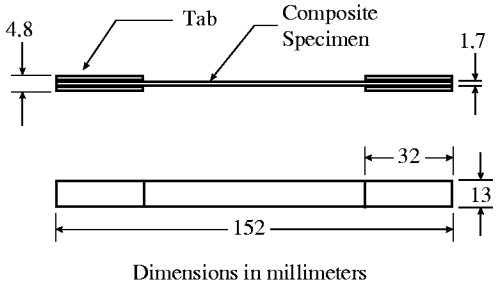

Figure 1. Flat straight sided specimen with bonded tabs.

temperature tests used the capacitive extensometers. The mechanical extensometer was manually calibrated such that 10 volts corresponded to 1.0 percent strain.

Tests were performed on a universal, digitally controlled, tensile testing frame with an electric actuator. They were conducted in the load control mode which provides a constant change in load with respect to time. The loading rate was fixed at 1.0 kN/min. (4.4 kips/min.). The 1.0 kN/min. (4.4 kips/min.) provides a fast enough strain rate for the specimen to limit the effects of creep and oxidation, but slow enough to manually monitor and respond to any problems (i.e. with gripping or extensometry) that may arise during a test. The load cell output was shunt calibrated with the output set at 20 kN equal to 10 V.

The specimen was loaded by passing it through the slot in the furnace then pulling the furnace between the grips while holding the specimen with tongs. The grips were clamped onto the specimen and the frame was placed in load control to maintain a no load condition. Next, the extensometer was inserted into the hot zone without contacting the specimen. The furnace was brought up to the desired test temperature at a rate of 30°C per minute (54°F/min.). Following stabilization of the test coupon temperature, the extensometer was brought into contact with the sample and the tensile test was started.

Once the tensile tests were completed several fractured composite specimens were observed with a scanning electron microscope (SEM) to determine the average matrix crack spacing. Matrix cracks and their locations within the gage length were recorded. The mean crack spacing and its standard deviation were determined.

5. Theory

Considerable effort has been applied to the mathematical modeling of the mechanical behavior of ceramic matrix composites. A complete understanding of the mechanical behavior of these composites is necessary if designers are to make use of them for high temperature engine applications. Important properties include the stiffness, first matrix cracking stress, ultimate strength, and work of fracture from room temperature to at least 1200°C.

5.1. Modulus

One of the basic properties of interest is the elastic modulus. The longitudinal Young's modulus of the composite is related to the matrix and fiber moduli, and their respective volume fractions by the rule of mixtures as presented in the following equation

$$E_c = V_f E_f + V_m E_m \tag{1}$$

where E is the modulus, V is the volume fraction, and subscripts c, f, and m refer to the composite, fiber, and matrix, respectively.

5.2. Matrix Cracking and Interfacial Shear Properties

In addition to studying the composite modulus, the proportional limit, in the direction of the fibers, needs to be investigated. It is assumed that the proportional limit on a stress/strain curve and the first matrix cracking stress are the same. This is a common assumption, as noted by Woodford and his associates (1993). The first matrix crack is taken by definition as the first through the cross section crack, wherein only the fibers are left to carry the total composite load. Any minor cracking within the composite before this condition or load is reached, is ignored in this definition. It is assumed that the fiber failure stress and strain are greater than the matrix failure stress and strain, respectively. The first matrix cracking stress is the onset of permanent major damage in a composite making it a critical design parameter. Shimansky (1989) describes the cracking process for CMCs with an increasing load as usually initiating with microcracks within an amorphous region at the fiber/matrix interface. The microcracks coalesce upon further increase in the applied load, forming major matrix cracks perpendicular to the loading axis that eventually traverse the whole composite cross-section. As the applied load continues to increase the matrix cracks at other points along the load axis. Finally, the matrix becomes saturated with regularly spaced parallel cracks. Once the composite matrix is saturated with cracks the remaining fiber/matrix interface area with each matrix segment is insufficient to transfer an adequate load to cause the matrix to fracture into smaller segments.

The first matrix cracking stress is dependent on many parameters. A key parameter is the fiber/matrix interfacial shear strength. Kerans (1989) has noted that the interfacial shear strength is difficult to characterize and may vary with location. In this work, the fiber/matrix interfacial shear strength is determined from matrix crack spacing measurements in a composite that has been loaded to or near its ultimate strength. Loading a specimen near the ultimate strength leads to matrix crack saturation. The average crack spacing for each specimen is used to determine the mean fiber/matrix interfacial shear strength, τ, using the equation

$$\tau = \frac{\beta \, R \, V_m \, E_m \, \sigma_y}{2 \, V_f \, E_c \, x} \tag{2}$$

where β=1.337 from Kimber and Keer (1982), R is the fiber radius, σ_y is the composite stress where matrix cracking initiates, and x is the length over which the additional load sustained by the fibers at the crack is transferred back to the matrix. This equation is derived from a summation of forces within the composite as presented by Aveston, et al. (1971). Aveston, et al. showed that the crack spacing is between x and 2x. Kimber and Keer (1982) demonstrated analytically that the crack spacing was closer to 1.337x. This equation is deterministic since it is assumed that the composite stress where matrix cracking initiates, that is σ_y, is constant.

In most composite systems there is a coefficient of thermal expansion (CTE) mismatch between the fibers and the matrix. This results in residual stresses within the composite at temperatures other than the processing temperature. The following equation from Budiansky, et al. (1986) is used to determine the axial residual stress within the matrix:

$$\sigma_{m\alpha} = \left[E_m \frac{\phi_2}{\phi_1} \right] \left[\frac{E_f}{E_c} \right] \left[\frac{V_f}{1 - \nu_m} \right] \varepsilon_T \tag{3}$$

where:

$$\varepsilon_T = (\alpha_f - \alpha_m)\Delta T \tag{4}$$

$$\Delta T = (T - T_{proc}) \tag{5}$$

$$\phi_1 = 1 - 0.5 \left[\frac{1 - 2\nu}{1 - \nu} \right] \left[1 - \frac{E_c}{E_f} \right] \tag{6}$$

$$\phi_2 = 0.5 \left[1 + \frac{E_c}{E_f} \right] \tag{7}$$

The variables α_f and α_m are the coefficients of thermal expansion for the fiber and matrix, respectively. The processing temperature is T_{proc} and the test temperature is T. The Poisson's ratio, ν, for the fiber and the matrix is assumed to be the same.

Aveston, et al. (1971) derived an equation for predicting the composite stress where matrix cracking initiates in brittle matrix composites. This is commonly referred to as the ACK theory and the result is presented in equation 8. The parameters include the fiber/matrix interfacial shear strength τ, the matrix fracture surface energy γ_m, the fiber radius R, the constituent volume fractions V, and constituent moduli E.

$$\sigma_y = \left[\frac{12 \tau \gamma_m E_c^2 E_f V_f^2}{E_m^2 V_m R} \right]^{\frac{1}{3}} \tag{8}$$

Note that the above equation is independent of crack size. It is a discrete model that was derived using an energy balance approach. The ACK theory uses the change in energy states within the composite from just prior to matrix crack initiation to just after the crack propagates completely through the matrix. Important assumptions included are: (1) the fiber failure strain is greater than the matrix failure strain, (2) a frictional interfacial bond between the fiber and the matrix exists, and (3) the fibers can bear the load without any support from the matrix.

Chawla (1993) pointed out some limitations or problems with the ACK theory. First, the theory indicates that the matrix strain to failure, or the first matrix cracking stress in equation 8, goes to zero as the fiber volume fraction goes to zero, whereas, the limit should be the strain or stress to failure of the monolithic matrix material. The model predicts that the strain to failure increases with increasing fiber/matrix interfacial shear strength. Unfortunately, the theory does not account for the limitation where fiber/matrix interfacial debonding and/or sliding does not occur. The lack of relative displacement at the fiber/matrix interface prevents fiber bridging of the matrix crack, resulting in linear elastic behavior.

Another equation for predicting the first matrix cracking stress was developed by Marshall and Cox (1988) using the crack closure pressure suggested by McCartney (1987). This approach was applied by Chulya, et al. (1991) to SiC/RBSN to calculate the first matrix cracking stress. Marshall and Cox (1988) used linear elastic fracture mechanics and assumed a single crack, loaded in mode I, propagating through a semi-infinite medium. The traction from the bridging fibers was superimposed on the crack model as closing pressure. The resulting equation is similar to the ACK results. Marshall and Cox also assumed a weak frictional fiber/matrix interface with bridging fibers. The resultant equation for predicting the composite stress where steady state matrix cracking begins within the lamina is

$$\sigma_y = \left[\frac{6\tau\gamma_m E_c^2 E_f V_f^2}{E_m^2 V_m R} \right]^{\frac{1}{3}} \tag{9}$$

Combining equations 3 and 9 leads to an equation which predicts the composite cracking stress with residual stress effects included. The result is

$$\sigma_{y\alpha} = \sigma_y - \sigma_{m\alpha} \frac{E_c}{E_m} \tag{10}$$

Danchaivijit and Shetty (1993) and Budiansky, et al. (1986) have pointed out that the ACK result, as well as equation 9 above, lead to lower bound predictions.

5.3. Fiber Properties

As mentioned earlier, ceramic matrix composites contain fibers that have a higher failure strain than the matrix. As a result, the composite's mechanical properties are fiber dominated near the material's ultimate strength. This section discusses the behavior of ceramic fibers in preparation for analyzing the ultimate strength of unidirectional composites.

Most brittle materials, including ceramic fibers, show a large variation in their tensile strength. Therefore, it is appropriate to apply statistical techniques for predicting their reliability and probability of failure. Statistical analysis allows the designer to use data generated from a small sample to systematically predict the stochastic response of complex structures.

Bergman (1984) reported that the cumulative distribution function proposed by Weibull (1939) is the most useful for characterization of brittle materials. Weibull analysis is based on the weakest link theory, where failure is assumed to occur at the largest flaw within the material. The sapphire fibers in this study consist of single crystals eliminating creep due to sliding grains but according to Bunsel and Berger (1997) the fibers are not without defects. Bunsel and Berger (1997) observed bubbles in the fibers most probably due to meniscus at the point of fiber growth and convection in the melt during fiber production. The Weibull theory is purely statistical in nature. It should be noted that a single flaw population and a strength that is independent of time will be assumed. The three parameter Weibull cumulative distribution function for the failure probability of ceramic fibers is

$$P_f = 1 - e^{-\int_V \left(\frac{\sigma - \sigma_t}{\sigma_0} \right)^m dV} \tag{11}$$

where P_f is the probability of failure by fracture at a given stress, σ, m is the shape factor, known as the Weibull modulus, V is the stressed volume, σ_0 is the scale factor, and σ_t is the location parameter defined as the threshold stress below which the probability of failure is zero. The scale factor, σ_0, has the dimension of stress times (volume)$^{1/m}$ for P_f to be dimensionless. The above equation can be simplified by taking the conservative assumption of setting the threshold stress to zero, assuming uniaxial fiber stress acting in a material volume with only internal imperfections. Consequently, equation 11 can be expressed as

$$P_f = 1 - e^{-V\left(\frac{\sigma}{\sigma_0} \right)^m} \tag{12}$$

The above equation is linearized by taking the natural logarithm twice, resulting in the following equation:

$$y = \ln\left[\ln\left(\frac{1}{1 - P_f} \right) \right] = \ln(V) + m \ln\left(\frac{\sigma}{\sigma_0} \right) \tag{13}$$

This equation can be plotted on a Weibull plot of y versus ln σ wherein the Weibull modulus, m, is the slope of the plotted line. The Weibull characteristic strength may be substituted for the volume and Weibull scale parameter to simplify the above equations. The Weibull characteristic strength, σ_θ, is a function of the Weibull scale parameter, σ_o; the stressed volume, V; and the Weibull modulus, m; as shown in the following equation:

$$\sigma_\theta = \frac{\sigma_o}{V^{\frac{1}{m}}} \tag{14}$$

Equation 14 is valid for the condition where the stress is evenly distributed over the volume, V, as is the case in uniaxial tension. Substituting equation 14 into equations 12 and 13 we get

$$P_f = 1 - e^{-\left(\frac{\sigma}{\sigma_\theta} \right)^m} \tag{15}$$

$$y = \ln\left[\ln\left(\frac{1}{1 - P_f} \right) \right] = m \ln\left(\frac{\sigma}{\sigma_\theta} \right) \tag{16}$$

Pai and Gyekenyesi (1988) and Mahfuz, et al. (1997) report that the least squares analysis and maximum likelihood method are the most popular techniques for estimating Weibull parameters from experimental data. The least squares method

offers simplicity with the estimated Weibull modulus being the slope of the best fit line by linear regression on a Weibull plot of y versus ln(σ). Bergman (1984) also states that the use of the least squares method implies that the ln σ values follow a Gaussian distribution around the line obtained from equation 13. The maximum likelihood technique is a nonlinear model offering efficiency and is better suited to model uniaxial strength data of brittle ceramics. ASTM (1995) has a standard (Designation: C 1239-94a) utilizing the maximum likelihood technique for estimating the Weibull parameters. The maximum likelihood method will be used for this work. The likelihood function, from the ASTM (1995) standard, for the two-parameter Weibull distribution, with a single-flaw population or uncensored data set is

$$L = \prod_{n=1}^{n_{tot}} \left(\frac{m}{\sigma_\theta}\right)\left(\frac{\sigma_n}{\sigma_\theta}\right)^{m-1} e^{-\left(\frac{\sigma_i}{\sigma_\theta}\right)^m} \tag{17}$$

where n is the rank of a specimen and n_{tot} is the total number of specimens in a sample.

The estimates of the Weibull modulus and the characteristic strength are determined by taking the partial derivatives of the natural logarithm of the likelihood function, equation 17, with respect to m and σ_θ and equating the resulting expressions to zero. Following are the resulting equations, for an uncensored sample, which are to be solved numerically.

$$\frac{\sum_{n=1}^{n_{tot}} \sigma_n^m \ln(\sigma_n)}{\sum_{n=1}^{n_{tot}} \sigma_n^m} - \frac{1}{n_{tot}} \sum_{n=1}^{n_{tot}} \ln(\sigma_n) - \frac{1}{m} = 0 \tag{18}$$

$$\sigma_\theta = \left[\left(\sum_{n=1}^{n_{tot}} \sigma_n^m\right)\frac{1}{n_{tot}}\right]^{\frac{1}{m}} \tag{19}$$

The ASTM (1995) standard, designation C 1239-94a, states that the estimated Weibull modulus tends to be statistically biased. The bias is a function of the sample size. The bias decreases as the sample size is increased. The ASTM (1995) standard, designation C 1239-94a, provides a table of unbiasing factors as a function of sample size.

A probability estimator is used to give the probability of failure for each failure stress. These probability values are used to calculate y for a given corresponding stress. The measured fracture strengths of the fibers are ranked in ascending order. The following estimator is used to calculate the failure probability:

$$P_n(\sigma_n) = \frac{n-0.5}{n_{tot}} \tag{20}$$

where n is the rank of the specimen data point and n_{tot} is the sample size. Other common probability estimators were discussed by Bergman (1984). The above

probability estimator, which gives an average value of the empirical density function about the corresponding stress, is most useful for small samples of less than 50 as discussed by Bergman (1984). Also, the probability estimator of equation 20 is part of the ASTM (1995) standard, mentioned above.

5.4. Ultimate Strength

The ultimate strength of the sapphire fiber reinforced polycrystalline alumina composites is primarily dependent on fiber properties. The strength properties of single crystal alumina fibers, as a function of temperature, were measured in separate tests.

A simple approximation for predicting the composite ultimate tensile strength utilizes the rule of mixtures and the mean fiber strength. For the unidirectional lamina, assuming that the in-situ fiber and the independent fiber strengths are identical and that the matrix carries no load, we have

$$\sigma_{cu} = V_f \sigma_{fu} \tag{21}$$

where: σ_{cu} - the composite ultimate strength
σ_{fu} - the mean fiber ultimate strength

It is further assumed here that all the fibers are intact until just prior to the composite ultimate loading.

The assumption of uniformly strong fibers would be the ideal situation, but in practice the fibers tend to fail sequentially starting with the weakest fiber, until the applied load cannot be supported leading to total fracture. Since the fibers are brittle and exhibit stochastic behavior, it is more appropriate to apply statistics to determine their ultimate strength. Duffy, et al. (1991) have pointed out that the strength distribution of the fibers needs to be incorporated into an analytical model for predicting the ultimate strength of the composite.

Equation 22 from Curtin, et al. (1993) and Curtin (1993) has been used to determine the composite's ultimate strength in terms of fiber properties.

$$\sigma_{cu} = V_f \left(\frac{2}{m+2} \right)^{\frac{1}{m+1}} \left(\frac{m+1}{m+2} \right) \left[\frac{\sigma_{fu}^m \tau L_f}{R \ln(2)} \right]^{\frac{1}{m+1}} \tag{22}$$

where: L_f - fiber gage length at which the strength was determined
m - Weibull modulus of fiber
σ_{fu} - mean fiber strength

It is of interest to compare the above result to that found for a “dry” bundle containing only fibers and no matrix. The composite strength based on bundle ultimate strength, σ_{cub}, can be calculated, per Evans, et al. (1995), from

$$\sigma_{cub} = V_f \sigma_{fu} \left(\frac{L_f}{L_c} \right)^{\frac{1}{m}} e^{-\frac{1}{m}} \tag{23}$$

where L_c is the fiber bundle gage length and L_f is the fiber length used to determine σ_{fu} and m. Equation 23 uses the rule of mixtures to estimate the composite strength, σ_{cub}, with the product of the fiber volume fraction and the fiber bundle strength, σ_{fub}.

Evans (1989), as well as Evans and Marshall (1989), presented a model for predicting the composite ultimate strength based on weakest link statistics, incorporating the fiber Weibull modulus, m. The model is a modified bundle failure analysis which assumes failed fibers have no load bearing ability. The model of the modified bundle failure theory is presented in the following equation:

$$\sigma_{cubm} = V_f \sigma_{fub} e^{-\frac{1-\left(1-\frac{\tau x}{R\sigma_{fub}}\right)^{m+1}}{(m+1)\left[1-\left(1-\frac{\tau x}{R\sigma_{fub}}\right)^{m}\right]}} \tag{24}$$

The fiber bundle strength, σ_{fub}, is determined by iteratively solving the following equation:

$$\left(\frac{R\sigma_{fub}}{\tau x} \right)^{m+1} = \frac{A_o}{2\pi R L_c} \left(\frac{R\sigma_o}{\tau x} \right)^{m} \left[1 - \left(1 - \frac{\tau x}{R\sigma_{fub}} \right)^{m} \right]^{-1} \tag{25}$$

where τ is the interfacial shear stress as defined by equation 2, x is the saturated matrix crack spacing, R is the fiber radius, L_c is the composite gage length, and A_o is an area normalizing factor. The scale parameter, σ_o, is defined, according to Chulya, et al. (1991), by the following equation:

$$\sigma_o = \frac{\sigma_{fu}}{\Gamma\left(1+\frac{1}{m}\right)} (2\pi R L_f)^{\frac{1}{m}} \tag{26}$$

Here L_f is the fiber gage length and Γ is Euler's gamma function, defined as:

$$\Gamma\left(1+\frac{1}{m}\right) = \int_0^\infty t^{\left(1+\frac{1}{m}\right)-1} e^{-t} dt \tag{27}$$

Cao and Thouless (1990) made an attempt to predict the ultimate strength of a ceramic composite with the application of two parameter Weibull statistics. Their theory assumed that the matrix is saturated with cracks. As a result, the initial linear elastic behavior and the nonlinear deformation associated with matrix cracking are not incorporated. Another simplifying assumption is that upon fracture of a fiber anywhere within the gage length of the composite, the fiber is unable to carry any

load. Given the assumptions, the following equation is used to predict the ultimate strength of a ceramic composite:

$$\sigma_{cu} = V_f \Sigma \left(\frac{\Sigma R}{m(m+1)\tau L_c} \right)^{\frac{1}{m}} e^{-\frac{1}{m}} \quad (28)$$

where:

$$\Sigma = \left[\frac{A_o \sigma_o^m \tau (m+1)}{2\pi R^2} \right]^{\frac{1}{m+1}} \quad (29)$$

As with the other theories in this section, this theory is based on fiber statistics, primarily the Weibull modulus and the scale parameter, and the variables are as defined in the statistical failure theories above.

6. Results and Discussion

In this section the high temperature tensile test results are presented and compared with theory to predict the mechanical behavior of the unidirectional fiber reinforced Al_2O_3/Al_2O_3 composite.

Table 1. High Temperature Mechanical Tensile Properties for Al_2O_3/Al_2O_3 Composites.

Specimen No.	T (°C)	E_c (GPa)	σ_y (MPa)	ε_y (%)	σ_{cu} (MPa)	ε_{cu} (%)
64a	22	146	274	0.190	425	0.400
64b	22	151	285	0.190	438	0.350
54a	22	167	308	0.190	362	0.320
54b	22	167	283	0.170	459	0.320
mean	**22**	**158**	**288**	**0.185**	**421**	**0.348**
std. dev.		11	14	0.010	42	0.038
SA167-1	800	168	142	0.080	149	0.082
SA167-2	800	138	206	0.135	206	0.135
SA167-3	800	152	147	0.092	147	0.092
mean	**800**	**153**	**165**	**0.102**	**167**	**0.103**
std. dev.		15	36	0.029	34	0.028
SA171-1	1000	108	47	0.452	89	0.047
SA171-2	1000	177	63	0.037	80	0.030
mean	**1000**	**143**	**55**	**0.245**	**84**	**0.039**
std. dev.		49	12	0.293	7	0.013
SA169-1	1200	128	84	0.054	84	0.054
SA169-2	1200	95	71	0.064	71	0.064
SA169-3	1200	110	103	0.080	103	0.080
mean	**1200**	**111**	**86**	**0.066**	**86**	**0.066**
std. dev.		17	16	0.013	16	0.013
SA180-1	1400	99	70	0.071	112	0.101
SA180-2	1400	106	74	0.071	120	0.097
SA180-3	1400	84	74	0.088	93	0.099
SA180-4	1400	106	52	0.047	95	0.027
mean	**1400**	**99**	**67**	**0.069**	**105**	**0.081**
std. dev.		10	11	0.017	13	0.036

T - test temperature
E_c – Young's modulus of composite
σ_y – first matrix cracking stress
ε_y – strain at first matrix cracking stress
σ_{cu} – ultimate strength of composite
ε_{cu} – strain at ultimate strength of composite

A typical stress-strain curve for the composite specimens is presented in Figure 2. All the specimens exhibited pseudo-toughness, or an ability to sustain progressive damage, from room temperature to 1400°C (2550°C) in air relative to monolithic polycrystalline alumina. These temperatures were selected to represent potential service conditions. All the specimens tested shared linear elastic behavior, followed by matrix cracking producing a limited nonlinear stress versus strain region. The measured mechanical properties for all the short term static tensile tests for the composite are presented in Table 1.

6.1. Modulus

Figure 3 and Table 1 show the Young's modulus of the composite as a function of temperature. The composite modulus decreases with increasing temperature. In

addition, Figure 3 illustrates the constituent moduli. The fiber moduli at 22°, 1000°, and 1400°C (72°, 1830°, and 2550°F) were provided by Dr. Ali Sayir (1998) of Case Western Reserve University. The high temperature fiber modulus data was generated using the system described by Sayir, et al. (1994). It can be observed in Figure 3 that the single crystal alumina fiber modulus varies fairly linearly with respect to temperature from room temperature to 1400°C (2550°F). This behavior is consistent with the observation made by Wachtman Jr. and Lam (1959) for single crystal alumina. Fiber moduli at 800° and 1200°C (1470° and 2190°F) were derived using linear interpolation.

Monolithic polycrystalline alumina specimens were tested at room temperature and 1200°C (2190°F). The room temperature results were reported by Jaskowiak and Setlock (1994). The material is the same as the matrix in the Al_2O_3/Al_2O_3 composite used for this work. The measured and interpolated moduli are presented in Figure 3. Wachtman Jr. and Lam (1959) showed that the modulus decreased linearly with respect to temperature from room temperature to approximately 950°C (1740°F). Above 950°C (1740°F) the modulus of the polycrystalline alumina dropped much more rapidly due to grain boundary softening and sliding according to Wachtman Jr. (1996). The percentage change in the modulus with respect to temperature presented by Wachtman Jr. and Lam (1959) was used to extrapolate moduli for the alumina used for the composite matrix at different temperatures.

The moduli of the constituents were used to determine the Young's modulus of the composite using the rule-of-mixtures, equation 1. The measured composite moduli and the calculated moduli are presented in Figure 3. There is excellent correlation between the measured and predicted values for the composite Young's modulus from room temperature to 1000°C (1830°F). At 1200°C (2190°F) the predicted value is greater than the mean measured modulus but within one standard deviation. Above 1400°C (2550°F) the rule of mixtures overestimates the modulus of the composite. The lower value of the measured Young's modulus at 1400°C (2550°F) may be due to changes in the zirconia interface between the fibers and the matrix. It is noted by Ryshkewitch and Richerson (1985) that the crystal structure of the zirconia starts to change from monoclinic to tetragonal at approximately 1000°C (1830°F) resulting in a volume reduction of about 9%. The volume reduction of the zirconia may be leading to debonding of the fiber/matrix interface. The fiber/matrix interfacial debonding would decrease or prevent load transfer between the fibers and the matrix which would reduce the fibers' contribution to the overall stiffness of the composite. A more in depth investigation of the interfacial properties at high temperatures may be a subject for future work.

6.2. Matrix Cracking and Interfacial Shear Properties

The effect of temperature on the proportional limit also was studied. It was assumed that the proportional limit, on a stress/strain curve, and the first matrix cracking stress were the same. The first matrix cracking stress is the onset of permanent damage in a composite, making it a critical design parameter.

The first matrix cracking stress is affected by various parameters. One of these parameters is the fiber/matrix interfacial shear strength. Other parameters are addressed later in this section. It has been noted by Kerans, et. al. (1989) that the interfacial shear strength is difficult to characterize with certainty. In this study the fiber/matrix interfacial shear strength is taken from the work of Jaskowiak, et al.

(1997) for room temperature. The high temperature interfacial shear stress is determined as a function of matrix crack spacing in a composite that has been loaded to the ultimate strength of the composite. Figure 4 illustrates the average matrix crack spacing as a function of temperature in air. Scatter was observed in the matrix crack spacing as indicated by the first standard deviation error bars in Figure 4. The matrix crack spacing was measured using a scanning electron microscope (SEM). It should be noted that it was very difficult to locate through-the-composite, fiber bridged, regularly spaced cracks within the Al_2O_3/Al_2O_3 composite. Next, the average crack spacing for each specimen was used to determine the mean fiber/matrix interfacial shear strength, τ, using equation 2. It is assumed that the matrix is characterized by a single value for strength. Yang and Knowles (1992) have made an attempt to apply Weibull statistics to characterize the matrix crack spacing with limited success, but more in depth analysis is required.

Table 2. Coefficients of Thermal Expansion for Sapphire Fibers and Polycrystalline Al_2O_3 Matrix.

T (°C)	α_f (10^{-6}/°C)	α_m (10^{-6}/°C)
22	6.26	6.03
800	8.43	7.90
100	8.72	8.14
1200	8.89	8.30
1400	9.02	8.43

α_f - fiber coefficient of thermal expansion

α_m - matrix coefficient of thermal expansion

Referring to Figure 4 it can be observed that matrix crack spacing decreases with increasing temperatures up to approximately 1200°C (2190°F). At 1400°C (2550°F) there is a significant increase in the matrix crack spacing. The large increase in matrix crack spacing may be attributed to a volume reduction of the zirconia at the fiber/matrix interface as discussed in the previous section, 6.1, on the modulus. The resultant debonding between the fibers and the matrix prevents the fibers from enhancing the matrix fracture stress relative to monolithic alumina. Figure 5 shows the interfacial shear strength as a function of temperature in air. It is difficult to conclude how the interfacial shear stress varies with temperature but there is a general reduction going from room temperature to 1400°C (2550°F). In addition, it may be noted that the interfacial shear strength is rather weak ranging from 55 to 3 MPa (8.0 to 0.4 ksi). The interfacial shear stress can vary significantly within a composite due to variations in processing conditions and effects of neighboring fibers as proposed by Chulya, Gyekenyesi, and Bhatt (1991). Research is continuing to identify a test for accurately determining the interfacial shear strength between the fiber and the matrix of various composite materials. This includes tensile tests of single fibers coated with the matrix material by Morscher, Martinez-Fernandez, and Purdy (1994) and fiber push-out tests by Eldridge, Bhatt, and Kiser (1991). Eldridge and Ebihara (1994) and Eldridge (1995) developed a high temperature fiber push-out system capable of testing specimens up to 1100°C (2010°F) in a vacuum environment.

The coefficient of thermal expansion (CTE) for the matrix and fibers are slightly different as can be observed in Table 2. The CTE values were taken from the work of Gitzen (1970) for 0° single crystal alumina and polycrystalline alumina. This results in residual stresses within the composite at temperatures other than the processing temperature. The processing temperature, assumed to be approximately 1300°C (2400°F), is used as the reference temperature at which there are no residual stresses due to the CTE mismatch within the composite. Equation 3 is used to determine the residual stress within the matrix. The Poisson's ratio is taken from the work of Gitzen (1970) and is assumed to be the same for the fiber and the matrix at a mean value of $\nu=\nu_f=\nu_m=0.22$.

The stress values at the proportional limit are illustrated in Figure 6 and Table 1. In addition, Figure 6 presents predicted values from the ACK theory and the Marshall and Cox theory combined with the McCartney theory. The matrix fracture surface energy, γ_m, is assumed to be a conservative 5 J/m^2 (0.03 $in \cdot lb_f/in^2$). The value for the matrix crack surface energy is taken from Wachtman Jr. (1996) who showed ceramics to typically vary from 5 to 50 J/m^2 (0.03 to 0.29 $in \cdot lb_f/in^2$).

Looking at Figure 6 and Table 1 we find that the estimated values for the first matrix cracking stress by the ACK theory (equation 8), and the Marshall and Cox theory combined with the McCartney theory (equation 9) were conservative at room temperature while not accounting for residual stresses and assuming a frictional fiber/matrix interface. By accounting for residual stresses the ACK theory estimates the room temperature first matrix cracking stress fairly accurately. On the other hand, by accounting for the residual stresses the Marshall and Cox theory combined with the McCartney theory still results in a conservative prediction for the first matrix cracking stress. Above room temperature all the theories over estimate the first matrix cracking stress. This is probably due to the difficulty in determining the fiber/matrix interfacial shear stress. In addition, the matrix fracture surface energy may be reduced slightly from the assumed value as temperature is increased. The ACK theory, with the assumption of a frictional fiber/matrix interface and not accounting for residual stresses, is recognized as a lower bound as pointed out by Danchaivijit and Shetty (1993) and Budiansky, Hutchinson, and Evans (1986), although, the Marshall-Cox theory combined with McCartney's theory, and not accounting for residual stresses, results in a more conservative prediction.

It should be noted that this study is primarily concerned with the high temperature behavior of these composites, that is, approximately at potential operating temperatures up to 1400°C (2550°F). Wachtman Jr. (1996) has shown that many researchers have observed a drop in strength between approximately 400° to 900°C (750° to 1650°F). Future studies of this composite system may be made in the lower temperature regime.

6.3. Sapphire Fiber Properties

The single crystal alumina fibers were tested in an "as-received" condition. That is, they were taken directly off the spool on which they were delivered and then tested.

The properties including the ultimate strength of individual fibers, mean ultimate strength with a variance of one standard deviation, Weibull modulus, and Weibull characteristic strength as a function of temperature for the sapphire fibers are presented in Table 3. In addition, the mean fiber ultimate strengths with one standard deviation are plotted as a function of temperature in Figure 7. Figure 8 presents a typical two-parameter Weibull plots with $Ln(Ln(1/(1-P_f))$ versus the fiber ultimate strength for the 'as-received' sapphire fibers. The same figure illustrates the 90% confidence bounds as determined using the ASTM (1995) standard designation C 1239-94a. Figure 9 presents the Weibull modulus as a function of temperature with 90% confidence bounds for the sapphire fibers.

The Weibull modulus is determined by numerically solving equations 18 and 19, which are part of the maximum likelihood method.

The data from Table 3 and Figure 7 indicate a steady decrease in ultimate strength with increasing temperature from room temperature to 1500°C (2730°F). Weibull moduli range from a low of 10 to a high of 24 from room temperature to

Table 3. The Ultimate Strength, Mean Ultimate Strength, Weibull Modulus, and Weibull Characteristic Strength as a Function of Temperature of Sapphire Fibers.

n	22°C σ_{fu} (GPa)	900°C σ_{fu} (GPa)	1000°C σ_{fu} (GPa)	1100°C σ_{fu} (GPa)	1200°C σ_{fu} (GPa)	1300°C σ_{fu} (GPa)	1400°C σ_{fu} (GPa)	1500°C σ_{fu} (GPa)
1	3.18	1.02	0.97	0.86	0.88	0.75	0.67	0.64
2	3.16	1.02	0.94	0.82	0.82	0.73	0.64	0.63
3	3.05	1.02	0.93	0.79	0.81	0.71	0.62	0.62
4	2.98	0.97	0.89	0.77	0.80	0.70	0.61	0.62
5	2.84	0.94	0.88	0.77	0.75	0.69	0.60	0.62
6	2.80	0.93	0.82	0.76	0.74	0.69	0.59	0.62
7	2.68		0.82	0.76	0.73	0.68	0.58	0.57
8	2.50		0.70	0.73	0.73	0.67	0.55	0.56
9	2.45		0.69	0.73	0.72	0.67	0.53	0.56
10	2.27			0.70	0.70	0.65	0.48	0.55
mean σ_{fu} (GPa) =	**2.79**	**0.99**	**0.85**	**0.77**	**0.77**	**0.69**	**0.59**	**0.60**
standard deviation	0.31	0.04	0.10	0.05	0.06	0.03	0.06	0.04
*m =	9.7	23.9	9.5	14.3	12.0	20.4	11.4	18.8
5% bound for m	6.2	13.1	6.0	9.2	7.7	13.1	7.4	12.1
95% bound for m	15.4	45.8	15.6	22.6	18.9	32.4	18.1	29.8
*σ_θ (GPa) =	2.91	1.00	0.89	0.79	0.79	0.71	0.61	0.61

environment: air
gage length: 25 mm
*Unbiased values derived by using maximum likelihood method with probability estimator $P=(n-0.5)/n_{tot}$ as per ASTM standard designation C 1239-94a
n - rank of the specimen data point
L_f - specimen gage length
m - Weibull modulus
σ_θ - characteristic strength

approximately 1500°C (2730°F) for the sapphire fibers. The scatter of the Weibull moduli as a function of temperature with the wide confidence bounds may be an indication that a larger sample of fibers is needed.

As noted in the section on matrix cracking, it should be pointed out that this study is primarily concerned with the high temperature behavior of these composites, that is, at potential operating temperatures up to approximately 1400°C (2550°F). Wachtman Jr. (1996) has shown that many researchers have observed a drop in strength between approximately 300° to 600°C (570° to 1110°F) for single crystal alumina. Future studies of this composite system may be made in the lower temperature regime.

7.1.4 Ultimate Tensile Strength of Al_2O_3/Al_2O_3

The ultimate strengths of these composites are primarily dependent on fiber properties. As a result, the mechanical properties of the composite, near the ultimate strength, will be effected by the environment in a similar manner as the fiber

constituent. The strength properties of the single crystal alumina fibers as a function of temperature were discussed in the previous section.

The ultimate tensile strengths of the composites are plotted as a function of temperature in Figure 10. The plot includes the mean ultimate strength with one standard deviation from tensile tests in air and theoretical curves using constituent properties. The same properties are presented in Table 4. To reiterate, the test temperatures were room temperature, 800°, 1000°, 1200°, and 1400°C. Figure 10 and Table 4 indicate a steady drop in the ultimate strength of the composite from room temperature to approximately 1000°C (1830°F). There is an almost insignificant increase in the ultimate strength from 1000°C (1830°F) to 1400°C (2550°F).

It can be observed in Figure 10 and Table 4 that the rule of mixtures, equation 21, over-predicts the ultimate strength considerably. It is only at 1400°C (2550°F) where the rule of mixtures prediction approaches the measured ultimate strength, but it is still higher than the experimentally observed values and the other theoretical predictions utilized in this section. It was mentioned in the previous chapter that this approach assumes that all the fibers are intact just prior to the composite ultimate strength. The rule of mixtures does not account for the brittle nature of the reinforcing fibers and the corresponding variance in the strength of the fibers. As a result, the rule of mixtures assumes ideal conditions, producing optimistic strength values relative to the experimentally derived measurements of the composites. Lastly, fiber damage, due to processing of the composite, may reduce the ultimate strength of the composite also.

Table 4. The Experimental and Theoretical Ultimate Tensile Strength of Al_2O_3/Al_2O_3 as a Function of Temperature in Air.

T (°C)	experimental (MPa)	ROM (MPa)	Curtin (MPa)	Evans 1995 (MPa)	Evans 1989 (MPa)	Cao & Thouless (MPa)
22	421±42	728	704	656	584	523
800	167±34	324	311	303	270	262
1000	84±7	227	209	205	173	170
1200	86±16	207	205	190	167	162
1400	105±13	182	159	167	145	142

experimental - mean and one standard deviation values from tensile tests
ROM - rule of mixtures
Curtin - Curtin's theory incorporating rule of mixtures and Weibull statistics with L_f=25 mm
Evans 1995 - Evans' theory using fiber bundle theory with no matrix material with L_f=L_c=25 mm except L_c=38 mm at room temperature
Evans 1989 - Evans' theory based on a modified fiber bundle theory
Cao & Thouless - Theory incorporating rule of mixtures and Weibull statistics
* Theoretical results using fiber properties in air

Since the fibers are brittle and exhibit linear elastic behavior with a significant variance in strength, relative to metals or other common structural materials, it is more appropriate to apply statistics to determine the ultimate strength. Curtin's (1993) theory, equation 22, incorporates Weibull statistics to address the variance in the strength of the fibers. Data from Figure 5 and Table 3 were used with Curtin's theory. The fiber gage length, L_f, is 25 mm (0.98). The results are presented in Table 4 and Figure 10. Curtin's theory also produces optimistic values for the ultimate strength. Unfortunately, the theory predicts strengths significantly over the measured

ultimate strengths. Curtin's theory is only a slight improvement over the simple rule of mixtures for predicting the ultimate strength of the brittle fiber reinforced Al_2O_3 composite system. As noted with the rule-of-mixtures, part of the discrepancy between Curtin's theory and the measured ultimate strength may be due to fiber damage during processing of the composites.

Evans, et al. (1995) tried to predict the ultimate strength of the composite using the rule of mixtures, the fiber bundle strength with Weibull statistics, and with the assumption that influence from the matrix was insignificant. The theory is presented in Equation 23. The results are shown in Figure 10 and Table 4. The mean fiber strengths and the fiber Weibull moduli were taken from Table 3. All gage lengths, L_f and L_c, are 25 mm except at room temperature where the composite gage length, L_c, assumed to be the same as the bundle gage length, is 38 mm. The theory overestimates the ultimate strength of the Al_2O_3/Al_2O_3 composite at all temperatures but it shows a similar curve to Curtin's theory. The curves show a reduction in ultimate strength from room temperature to approximately 1000°C (1830°F) with a minimal change 1000°C (1830°F) to 1400°C (2550°F). Again, fiber damage due to processing may add to the discrepancy between the theory of Evans, et al. (1995) and the measured composite ultimate strengths.

Evans (1989) presented a model based on a modified fiber bundle theory. The theory is presented in equation 24. The results are presented in Figure 10 and Table 4. The required parameters of the fiber bundle strength, σ_{fub}, was solved iteratively using equation 25 and the scale parameter, σ_o, was determined using equation 26. The area normalizing factor, A_o, was equal to 1.0 m^2. All gage lengths, L_f and L_c, are set at 25 mm (0.98 in.) except at room temperature where L_c=38 mm (1.5 in.). The theory produces results which are better than Curtin's theory (1993); Evans', et al. (1995) theory; and the rule of mixtures. At room temperature the prediction is 39% greater than the experimentally derived data. Unfortunately, the Evans' modified fiber bundle theory over predicts by up to 106% over the measured ultimate strength at 800°C (1470°F). Fiber degradation, due to the processing conditions of the composite, may have added to the discrepancy between the theory and the measured composite ultimate strength.

Cao and Thouless (1990) also presented a theory for predicting the ultimate strength for a ceramic composite. It is based on two parameter Weibull statistics as described in the previous section. The theory was applied to the Al_2O_3/Al_2O_3 system with the results presented in Figure 10 and Table 4. The same scale parameters, σ_o, calculated for the modified fiber bundle theory of Evans (1989), were used for this theory. The composite gage length, L_c, is set at 38 mm (1.5 in.) for room temperature and 25 mm (0.98 in.) for temperatures greater than room temperature. At room temperature, the theory over predicted the composite ultimate strength by 24%. The theoretical predictions over estimate the ultimate strength up to 102% at 1000°C (1830°F). Of the theories evaluated in this paper, the theory from Cao and Thouless (1990) does offer the best predictions for the composite ultimate strength but the results are still overly optimistic relative to the experimentally derived ultimate strengths. The theory provides similar predictions to the Evans' (1989) theory for temperatures between 800°C (1470°F) to 1400°C (2550°F). Composite fabrication induced fiber damage may have reduced the measured composite ultimate strength also.

All the theories that were addressed in this section using the fiber properties overestimated the ultimate strength of the Al_2O_3/Al_2O_3 composite. It was noted with each of the theories that the lower values of the experimentally obtained ultimate

strength measurements for the Al_2O_3/Al_2O_3 composite may be due to fiber damage incurred during processing of the Al_2O_3/Al_2O_3 or due to possible surface damage produced upon matrix fracture during the tensile test. Although as the test temperatures approach 1000°C (1830°F) and over, it is believed that the fiber strength degrades due to dislocation microplasticity, twinning, stresses due to thermal expansion anisotropy, and slow crack growth as noted by Wachtman Jr. (1996) for single crystal alumina. This degradation of intrinsic strength becomes more significant than the strength reduction due to surface damage. As a result, the predicted composite ultimate tensile strength, based on fiber properties, becomes more accurate when compared with the measured composite ultimate tensile strength. The application of the mean fiber strength and the fiber Weibull modulus does predict the ultimate strength of the composite with increased accuracy. Increasing the number of specimens per test should show more accurate results when applying statistics. In addition, a more accurate technique is needed to model the fiber damage due to the processing of the composite. Lastly, the mean strengths and Weibull moduli for the fibers were generated by testing individual fibers. Hill and Okoroafor (1995) have observed a reduction in strength of fiber bundles due to inter-fiber friction. This inter-fiber friction may be causing some of the reduction in strength of the experimentally derived composite data relative to the theoretical values derived from individually tested fibers. On an interesting note, Cox, Marshall, and Thouless (1989) found that the fracture of composites is not greatly influenced by the breadth of the fiber strength distribution. Although the theories incorporating the scatter in fiber strength improved the predictions of the composite ultimate strength, the conclusions of Cox, Marshall, and Thouless (1989) reinforces the idea that the lower strength of composites is most likely due to damaged fibers caused by the processing conditions of the composite.

7. Summary and Conclusion

The composite system studied includes uniaxial single crystal alumina fiber reinforced polycrystalline alumina utilizing a porous ZrO_2 fiber/matrix interface. The Al_2O_3/Al_2O_3 composite was tensile tested at high temperatures in air from room temperature to 1400°C (2550°F).

The composite exhibited progressive fracture at all the test temperatures of the short term static tensile tests. The Young's modulus shows a slight decrease as the test temperature was increased from room temperature to 1000°C (1830°F) but decreased at a greater rate above 1000°C (1830°F). The rule of mixtures gives a good approximation of the Al_2O_3/Al_2O_3 modulus as function of temperature using the constituent moduli up to approximately 1200°C (2190°F). More information is required for predicting composite modulus above 1200°C (2190°F).

The characterization of the fiber/matrix interfacial shear strength requires further study. The first matrix cracking stress decreases with respect to temperature from room temperature to 1000°C (1830°F) followed by a slight increase up to approximately 1200°C (2190°F). The first matrix cracking stress continues to decrease as temperature is increased from 1200°C (2190°F) to 1400°C (2550°F). The ACK theory (1971), with the assumption of a frictional fiber/matrix interface and accounting for residual stresses, produces a good approximation for the composite first matrix cracking stress at room temperature. Above the room temperature the ACK theory and the Marshall and Cox theory combined with the McCartney theory

significantly overestimate the first matrix cracking stress whether the residual stresses are accounted for or not. This is believed to be, primarily, due to the difficulty in characterizing the fiber/matrix interfacial sheer stress above room temperature.

The ultimate strength of the composite showed a drop from room temperature to approximately 1000°C (1830°F) followed by a negligible increase in strength from 1000°C (1830°F) to 1400°C (2550°F). The theory of Cao and Thouless (1990) produced the best estimates of the composite ultimate strength relative to the theories evaluated in this work. Unfortunately, the Cao and Thouless theory over estimates the composite ultimate strength from 24 to 102% relative to the experimental values. There is a need to study the effects of composite processing on the fiber properties.

References

American Society for Testing and Materials, "ASTM Designation: C 1239-94a: Standard Practice for Reporting Uniaxial Strength Data and Estimating Weibull Distribution Parameters for Advanced Ceramics," 1995 Annual Book of ASTM Standards, Refractories; Carbon and Graphite Products; Activated Carbon; Advanced Ceramics. Vol. 15.01. ASTM, Philadelphia, PA.

American Society for Testing and Materials, "ASTM Designation: C 1359-96: Standard Test Method for Monotonic Tensile Strength Testing of Continuous Fiber-Reinforced Advanced Ceramics With Solid Rectangular Cross-Section Specimens at Elevated Temperatures." ASTM, Philadelphia, PA.

Aveston, J., Cooper, G. A., and Kelly, A., "Single and Multiple Fracture in the Properties of Fiber Composites," Conference Proceedings, National Physical Laboratory, Guilford. IPC Science and Technology Press Ltd., Surrey, England, 1971, pp. 15-26.

Bergman, B., "On the Estimation of the Weibull Modulus," Journal of the Materials Science Letters, Vol. 3, 1984.

Budiansky, B., Hutchinson, J. W., and Evans, A. G., "Matrix Fracture In Fiber Reinforced Ceramics," Journal of the Mechanics and Physics of Solids, Vol. 34, 1986, pp. 167-189.

Bunsell, A. R. and Berger, M. H., "Ceramic Fiber Development and Characterization," Key Engineering Materials, Vols. 127-131, 1997, pp. 15-26.

Cao, H. and Thouless, M. D., "Tensile Tests of Ceramic-Matrix Composites: Theory and Experiment," Journal of the American Ceramic Society, Vol. 73, No. 7, 1990.

Chawla. K. K., Ceramic Matrix Composites. London: Chapman and Hall, 1993.

Chulya, A., Gyekenyesi, J. P., and Bhatt, R. T., "Mechanical Behavior of Fiber Reinforced SiC/RBSN Ceramic Matrix Composites: Theory and Experiment," NASA Technical Memorandum 103688, 1991.

Constance, J., "Industry Turns to Ceramic Composites," Aerospace America, Mar., 1990.

Cox, B. N., Marshall, D. B., and Thouless, M. D., "Influence of Statistical Fiber Strength Distribution on Matrix Cracking in Fiber Composites," Acta Metallurgica, Vol. 37, No. 7, 1989, pp. 1933-1943.

Curtin, W. A., Eldridge, J. I., and Srinivasan, G. V., "New Silicon Carbide/Reaction Bonded Silicon Carbide Ceramic Matrix Composite," Journal of the American Ceramic Society, Vol. 76, No. 9, 1993.

Curtin, W. A., "Ultimate Strengths of Fibre-Reinforced Ceramics and Metals," Composites, Vol. 24, No. 2, 1993.

Danchaivijit, S. and Shetty, D. K., "Matrix Cracking In Ceramic-Matrix Composites," Journal of the American Ceramic Society, Vol. 76, No. 10, 1993.

Dev, S. P., "Emerging Technologies for Gas Turbine Engines: U.A.V. Synergies," American Institute of Aeronautics and Astronautics report AIAA-92-3757, 1992.

Dix, D. M. and Petty, J. S., "Aircraft Technology Gets A Second Wind," Aerospace America, Jul., 1990.

Drascovich, B. S., "Fibers for Turbines," CFCC News, Summer, 1993.

Duffy, S. F., Chulya, A., and Gyekenyesi, J. P., "Structural Design Methodologies for Ceramic-Based Material Systems," NASA Technical Memorandum 103097, 1991.

Duffy, S. F. and Gyekenyesi, J. P., "Reliability and Life Prediction of Ceramic Composite Structures at Elevated Temperatures," in High Temperature Mechanical Behavior of Ceramic Composites, S.V. Nair and K. Jakus, eds., pp. 471-515, Butterworth-Heinemann, Boston, 1995.

Eldridge, J. I., Bhatt, R. T., and Kiser, J. D., "Investigation of Interfacial Shear Strength In SiC/Si_3N_4 Composites," NASA Technical Memorandum 103739, 1991.

Eldridge, J. I. and Ebihara, B. T., "Fiber Push-Out Testing Apparatus For Elevated Temperatures," Journal of Materials Research, Vol. 9, No. 4, Apr., 1994.

Eldridge, J. I., "Elevated Temperature Fiber Push-Out Testing," Mat. Res. Soc. Symp. Proc., Vol. 365, 1995, pp. 283-290.

Evans, A. G., "The Mechanical Performance of Fiber-Reinforced Ceramic Matrix Composites," Materials Science and Engineering, A107, 1989.

Evans, A. G. and Marshall, D. B., "The Mechanical Behavior of Ceramic Matrix Composites," Acta Metallurgica, Vol. 37, No. 10, 1989, pp. 2567-2583.

Evans, A. G., Zok, F. W., and Mackin, T. J., "The Structural Performance of Ceramic Matrix Composites," High Temperature Mechanical Behavior of Ceramic Composites, ed. Nair, S. V. and Jakus, K., Boston: Butterworth-Heinemann, 1995, pp. 3-84.

Gitzen, W. H., Alumina As a Ceramic Material, The American Ceramic Society, Westerville, OH, 1970.

Gyekenyesi, J. Z., "High Temperature Mechanical Characterization of Ceramic Matrix Composites," Ph.D. Thesis, Cleveland State University, 1998.

Hill, R. and Okoroafor, E. U., "Weibull Statistics Of Fibre Bundle Failure Using Mechanical and Acoustic Emission Testing: The Influence of Interfibre Friction," Composites, Vol. 26, No. 10, 1995.

Holmes, J.W. and Wu, X., "Elevated Temperature Creep Behavior of Continuous Fiber-Reinforced Ceramics," in High Temperature Mechanical Behavior of Ceramic Composites, ed. Nair, S. V. and Jakus, K., pp. 193-259, Butterworth-Heinemann, Boston, 1995.

Jaskowiak, M. H., Eldridge, J. I., Setlock, J. A., and Gyekenyesi, J. Z., "Mechanical Behavior of Sapphire Reinforced Alumina Matrix Composites at Elevated Temperatures," The 21st Annual Conference on Ceramic, Metal, and Carbon Composites, Materials, and Structures, Parts 1 and 2, ed. Opeka, M. M., Jan. 26-31, 1997, pp. 123-136.

Jaskowiak, M. H. and Setlock, J. A., "Processing and Mechanical Properties of Sapphire Reinforced Alumina Matrix Composites," Presented at the 7th Annual HITEMP Review, Cleveland, OH, Oct., 1994. NASA Conference Publication 10146.

Kerans, R. J., Hay, R. S., Pagano, N. J., Parthasarathy, T. A., "The Role of the Fiber-Matrix Interface in Ceramic Composites," Ceramic Bulletin, Vol. 68, No. 2, 1989.

Kimber, A. C. and Keer, J. G., "On the Theoretical Average Crack Spacing In Brittle Matrix Composites Containing Continuous Aligned Fibers," Journal of Materials Science Letters, Vol. 1, 1982.

King, J. E., "Failure In Composite Materials," Metals and Materials, Dec., 1989.

Levine, S. R., "Ceramics and Ceramic Matrix Composites - Aerospace Potential and Status," American Institute of Aeronautics and Astronautics report AIAA-92-2445-CP, 1992.

Mahfuz, H., Maniruzzaman, Md., Vaidya, U., Brown, T., Jeelani, S., "Response of SiC_f/Si_3N_4 Composites Under Static and Cyclic Loading-An Experimental and Statistical Analysis," Transactions of the ASME, Vol. 119, Apr., 1997.

Marshall, D. B. and Cox, B. N., "A J-Integral Method for Calculating Steady-State Matrix Cracking Stresses In Composites," Mechanics of Materials, Vol. 7, 1988, pp. 127-133.

McCartney, L. N., "Mechanics of Matrix Cracking in Brittle-Matrix Fiber-Reinforced Composites," Royal Society of London, Proceedings, Series A, Vol. 409, 1987, pp. 329-350.

Morscher, G. N., Martinez-Fernandez, J., and Purdy, M. J., "Determination of Interfacial Properties Using a Single Fiber Microcomposite Test," Presented at the 96th Annual American Ceramic Society Meeting, Apr. 24-27, 1994, Indianapolis, IN.

Pai, S. S. and Gyekenyesi, J. P., "Calculation of Weibull Strength Parameters and Batdorf Flaw-Density Constants for Volume- and Surface-Flaw-Induced Fracture in Ceramics," NASA Technical Memorandum 100890, 1988.

Ryshkewitch, E. and Richerson, D. W., Oxide Ceramics, Orlando, FL: Academic Press, Inc., 1985.

Sayir, A., Personal communication, NASA Lewis Research Center, Aug., 1998.

Sayir, A., Greer III, L. C., Goldsby, J. C., Oberle, L. G., "Laser Speckle Micro-Strain Measurements On Small Diameter Fibers," Ceramic Engineering and Science Proceedings, Vol. 15, Nos. 4, 1994, pp. 397-409.

Sheppard, L. M., "Enhancing Performance of Ceramic Composites," Ceramic Bulletin, Vol. 71, No. 4, 1992.

Shimansky, R. A., "Effect of Interfaces On Continuous Fiber-Reinforced Brittle Matrix Composites," Ann Arbor, Michigan: University Microfilms International, 1989.

Studt, T., "Breaking Down Barriers for Ceramic Matrix Composites," R&D Magazine, Aug., 1991.

Taylor, R., "Ceramic Fiber/Ceramic Matrix Composites - Why and How?" SAMPE Journal, Vol. 27, No. 4, Jul./Aug., 1991.

Wachtman Jr., Mechanical Properties of Ceramics, New York: John Wiley & Sons, Inc., 1996.

Wachtman Jr., J. B. and Lam Jr., D. G., "Young's Modulus of Various Refractory Materials as a Function of Temperature," Journal of the American Ceramic Society, Vol. 42, No. 5, 1959, pp. 254-260.

Warren, R., "Overview," Ceramic-Matrix Composites. ed. R. Warren. New York: Chapman and Hall, 1992. p.5

Weibull, W., "The Phenomenon of Rupture in Solids," Ingeniors Ventenskaps Akademien Handlinger, No. 153, 1939, pp. 5-55.

Woodford, D. A., Van Steele, D. R., Brehm, J. A., Timms, L. A., and Palko, J. E., "Testing the Tensile Properties of Ceramic-Matrix Composites," JOM, Vol. 45, No. 5, May, 1993.

Worthem, D. W. and Lewinsohn, "Effect of Specimen Design on the Tensile Properties of Ceramic Matrix Composites," Presented at the 4th Annual HITEMP Review, Cleveland, OH, Oct., 1991. NASA Conference Publication 10082.

Yang, X. F. and Knowles, K. M., "The One-Dimensional Car Parking Problem and Its Application to the Distribution of Spacings Between Matrix Cracks In Unidirectional Fiber-Reinforced Brittle Materials," Journal of the American Ceramic Society, Vol. 75, No. 1, 1992, pp. 141 147.

Yoshida, M. and Kokaji, A., "Firing Up the Future with Ceramic Engine Parts," Machine Design, Oct. 26, 1989.

Zweben, C., "Advanced Composites In Spacecraft and Launch Vehicles," Launchspace, Jun./Jul., 1998.

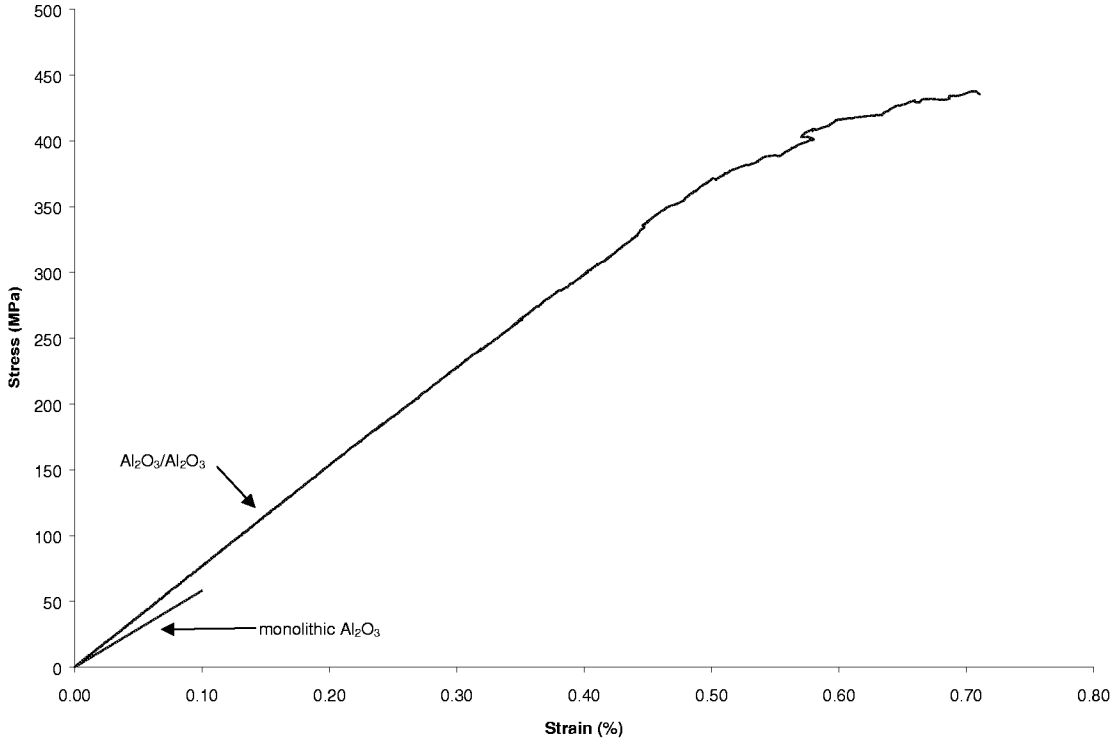

Figure 2. Typical tensile stress-strain curve for unidirectional Al_2O_3/Al_2O_3 composites with approximately 27% fiber volume fraction and monolithic Al_2O_3.

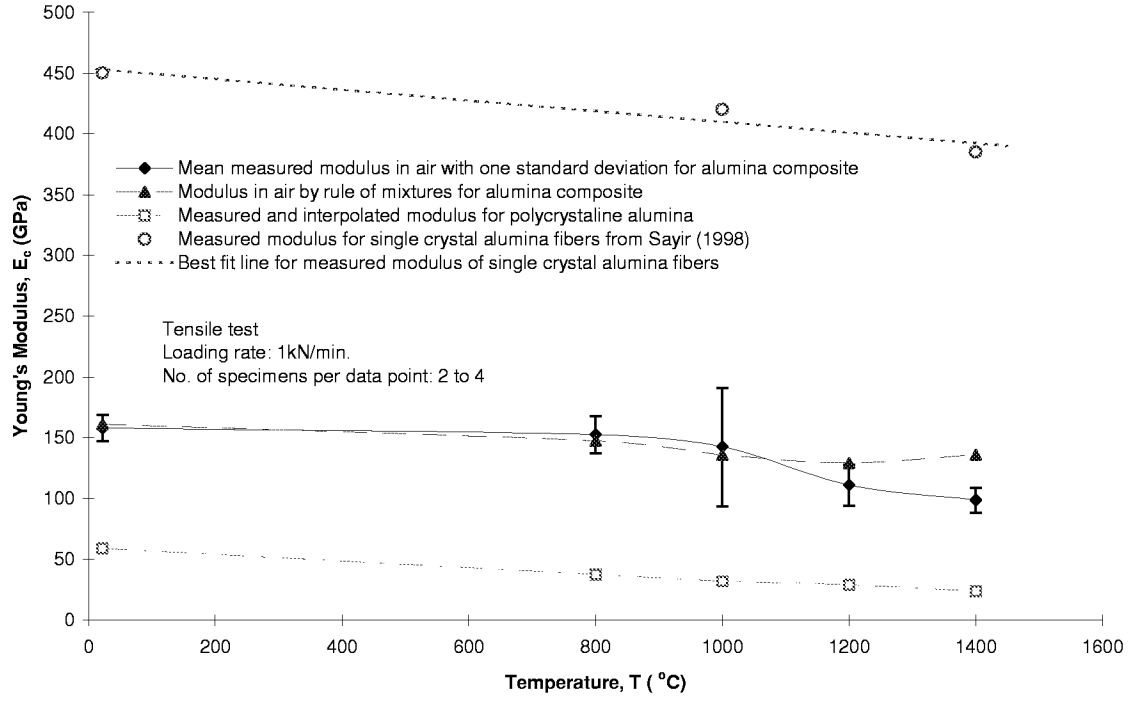

Figure 3. Tensile Young's modulus of Al_2O_3/Al_2O_3 composite, sapphire fiber, and monolithic Al_2O_3 vs. temperature. The mononlithic polycrystalline Al_2O_3 has approximately the same porosity as the matrix in the composite.

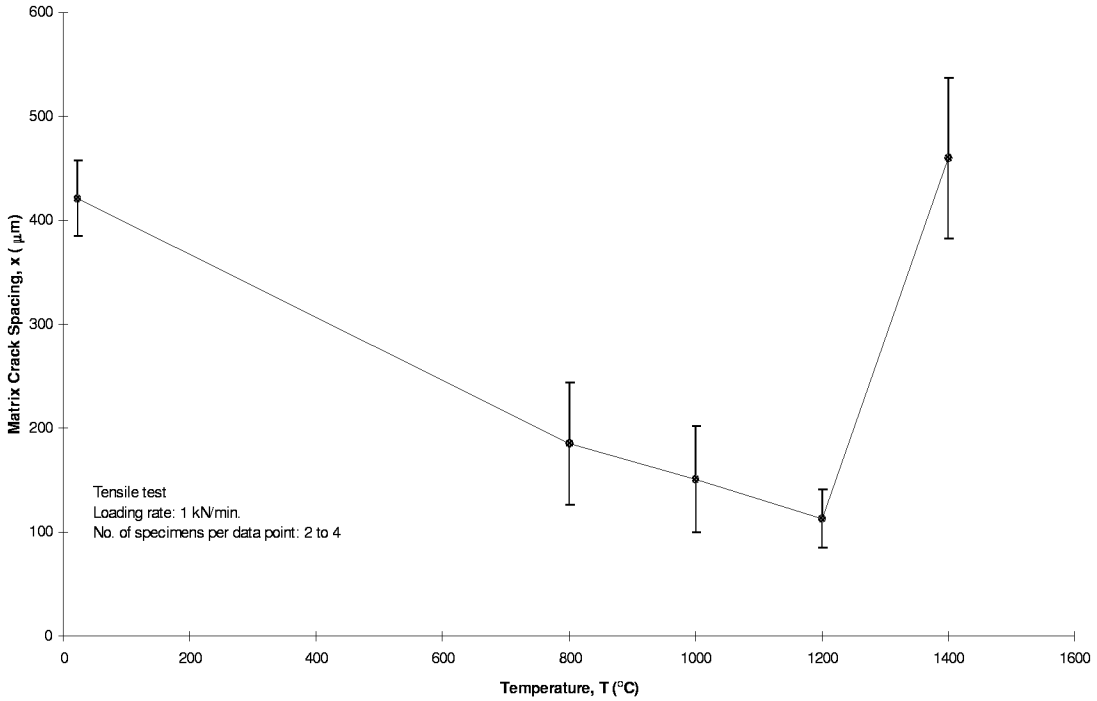

Figure 4: Mean matrix crack spacing with one standard deviation versus temperature in air for unidirectional Al_2O_3/Al_2O_3 composites when loaded in the primary direction.

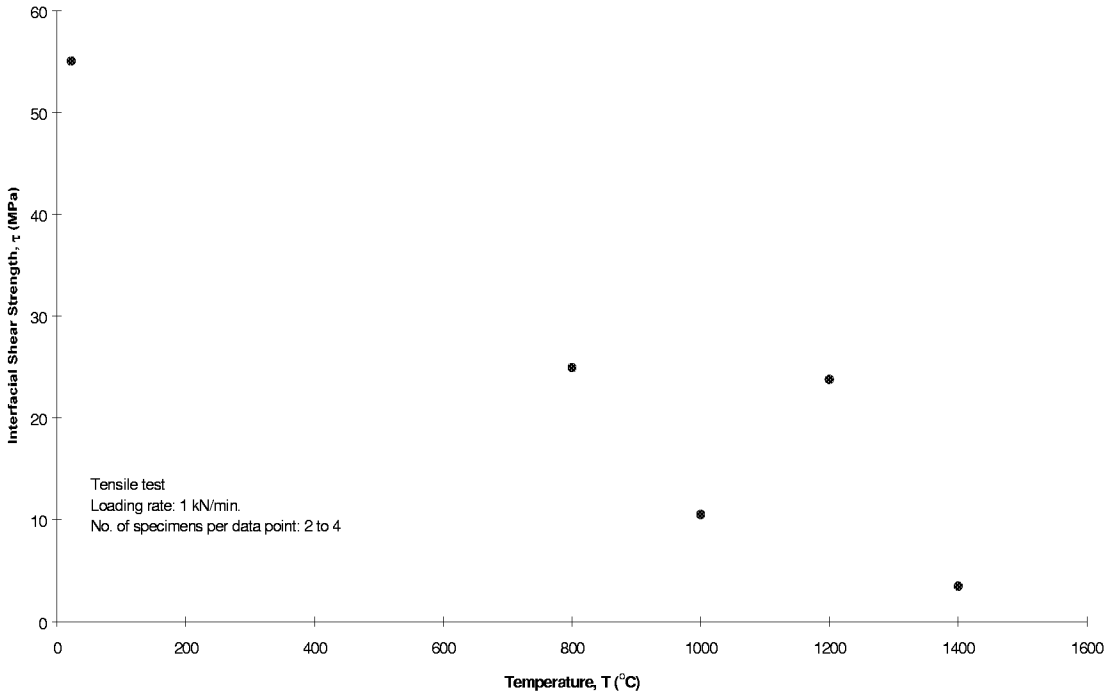

Figure 5. Fiber/matrix interfacial shear strength versus temperature in air for Al_2O_3/Al_2O_3 composites.

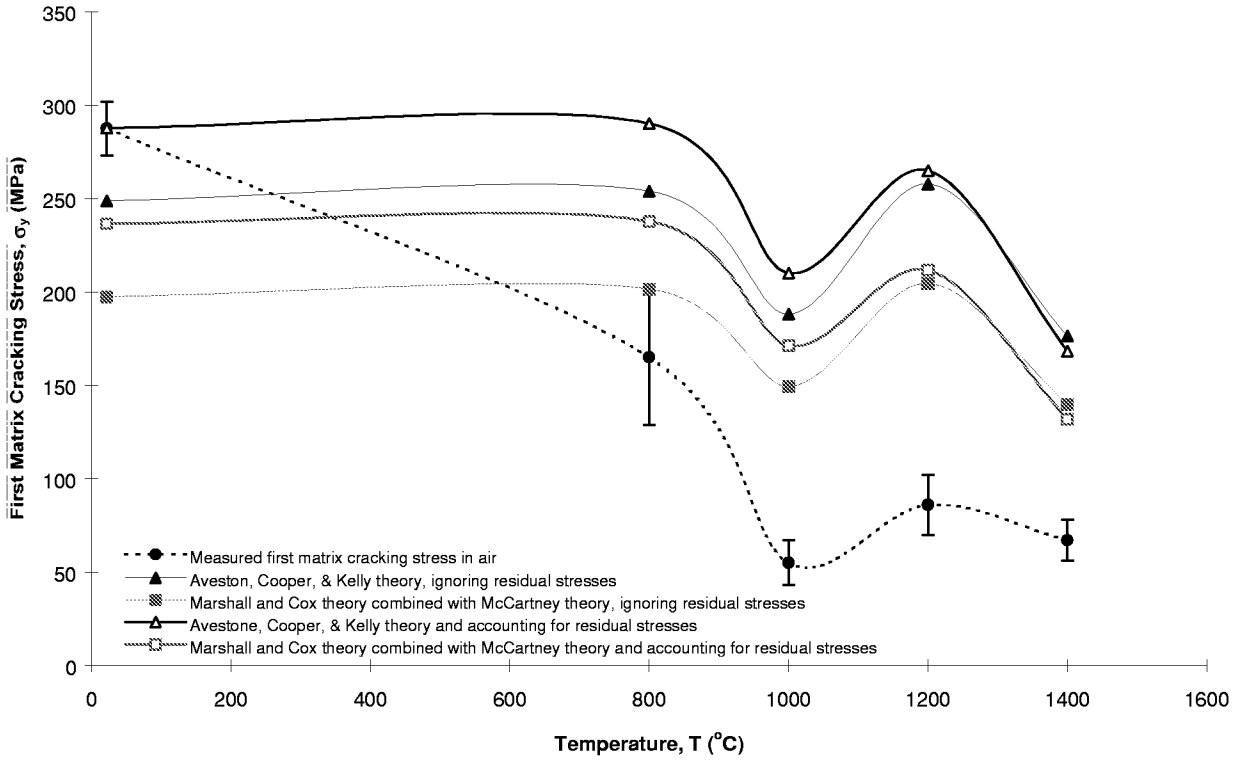

Figure 6. Average with one standard deviation, measured and predicted unidirectional Al_2O_3/Al_2O_3 composite tensile first matrix cracking stresses as a function of temperature in air. Loading was along the primary direction.

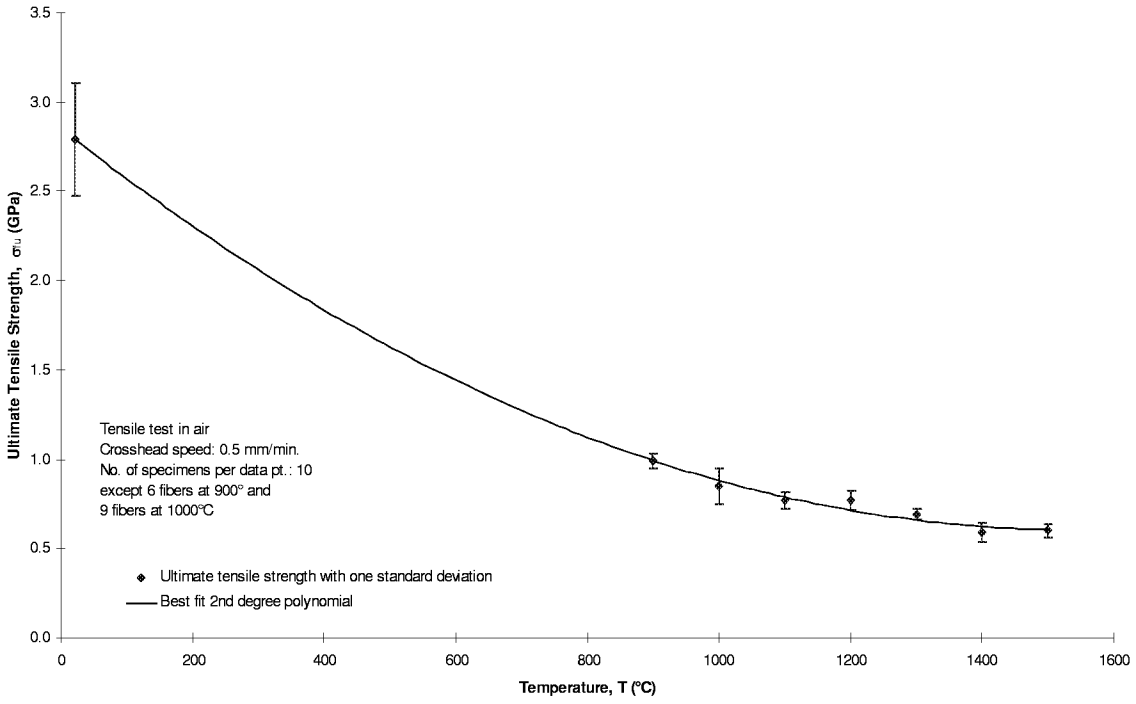

Figure 7. Mean ultimate tensile strength with one standard deviation of single crystal alumina fibers as a function of temperature in air.

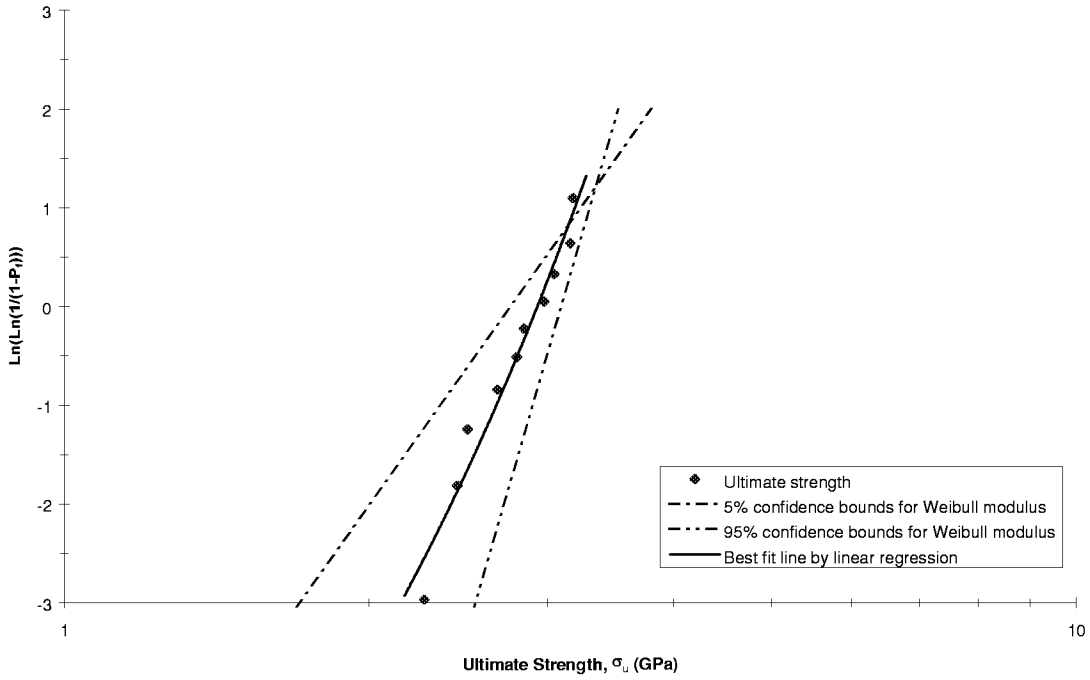

Figure 8. A typical plot for Ln(Ln(1/(1-P_f))) versus the ultimate tensile strength of individual single crystal alumina fibers. Ninety percent confidence bounds determined as per ASTM (1995) standard designation C 1239-94a.

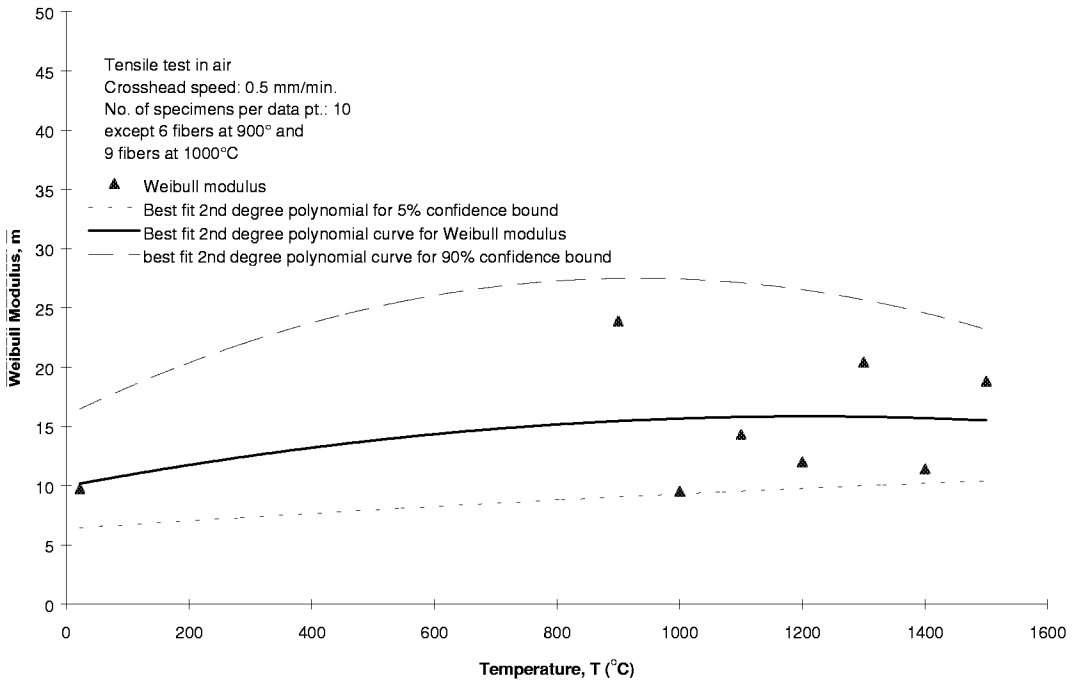

Figure 9. Weibull modulus of single crystal alumina fibers as a function of temperature in air.

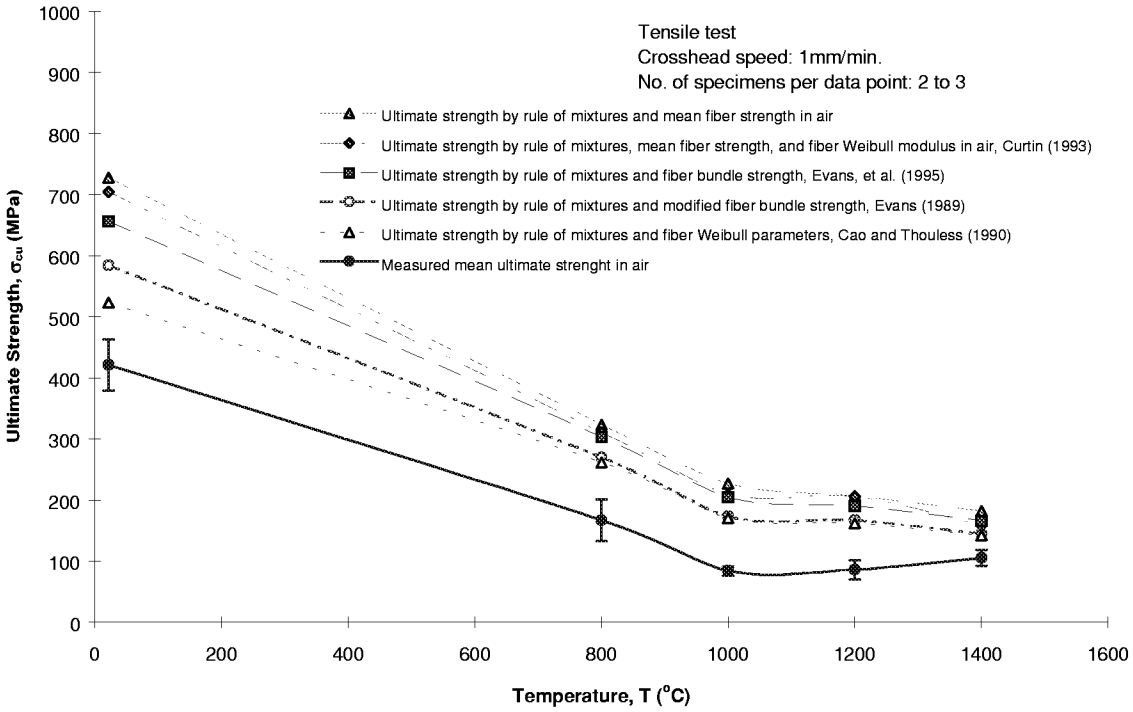

Figure 10. Average measured Al_2O_3/Al_2O_3 composite ultimate tensile strength with one standard deviation relative to predictions of the composite ultimate strength using single crystal alumina fiber properties as a function of temperature. Loading was along the primary direction.

REPORT DOCUMENTATION PAGE

Form Approved
OMB No. 0704-0188

1. AGENCY USE ONLY (*Leave blank*)	2. REPORT DATE	3. REPORT TYPE AND DATES COVERED
	February 1999	Technical Memorandum

4. TITLE AND SUBTITLE

High Temperature Mechanical Characterization and Analysis of $A1_2O_3/A1_2O_3$ Composition

5. FUNDING NUMBERS

WU–523–21–13–00

6. AUTHOR(S)

John Z. Gyekenyesi and Martha H. Jaskowiak

7. PERFORMING ORGANIZATION NAME(S) AND ADDRESS(ES)

National Aeronautics and Space Administration
Lewis Research Center
Cleveland, Ohio 44135–3191

8. PERFORMING ORGANIZATION REPORT NUMBER

E–11562

9. SPONSORING/MONITORING AGENCY NAME(S) AND ADDRESS(ES)

National Aeronautics and Space Administration
Washington, DC 20546–0001

10. SPONSORING/MONITORING AGENCY REPORT NUMBER

NASA TM—1999-208855

11. SUPPLEMENTARY NOTES

John Z. Gyekenyesi, University of Akron, Civil Engineering Department, Akron, Ohio 44325 (work funded under NCC3–615); and Martha H. Jaskowiak, NASA Lewis Research Center. Responsible person, Martha H. Jaskowiak, organization code 5130, (216) 433–5515.

12a. DISTRIBUTION/AVAILABILITY STATEMENT

Unclassified - Unlimited
Subject Categories: 39 and 27 Distribution: Nonstandard

This publication is available from the NASA Center for AeroSpace Information, (301) 621–0390.

12b. DISTRIBUTION CODE

13. ABSTRACT ***(Maximum 200 words)***

Sixteen ply unidirectional zirconia coated single crystal Al_2O_3 fiber reinforced polycrystalline Al_2O_3 was tested in uniaxial tension at temperatures to 1400 °C in air. Fiber volume fractions ranged from 26 to 31%. The matrix has primarily open porosity of approximately 40%. Theories for predicting the Young's modulus, first matrix cracking stress, and ultimate strength were applied and evaluated for suitability in predicting the mechanical behavior of Al_2O_3/Al_2O_3 composites. The composite exhibited pseudo tough behavior (increased area under the stress/strain curve relative to monolithic alumina) from 22° to 1400 °C. The rule-of-mixtures provides a good estimate of the Young's modulus of the composite using the constituent properties from room temperature to approximately 1200 °C for short term static tensile tests in air. The ACK theory provides the best approximation of the first matrix cracking stress while accounting for residual stresses at room temperature. Difficulties in determining the fiber/matrix interfacial shear stress at high temperatures prevented the accurate prediction of the first matrix cracking stress above room temperature. The theory of Cao and Thouless, based on Weibull statistics, gave the best prediction for the composite ultimate tensile strength.

14. SUBJECT TERMS

Mechanical characterization; Alumina/alimina composite; Analytical modeling

15. NUMBER OF PAGES

36

16. PRICE CODE

A03

17. SECURITY CLASSIFICATION OF REPORT	18. SECURITY CLASSIFICATION OF THIS PAGE	19. SECURITY CLASSIFICATION OF ABSTRACT	20. LIMITATION OF ABSTRACT
Unclassified	Unclassified	Unclassified	